Surface & Coatings Technology 241 (2014) 159–167

Contents lists available at ScienceDirect

Surface & Coatings Technology

journal homepage: www.elsevier.com/locate/surfcoat

Design and optimisation of process parameters in an in-line CIGS evaporation pilot system ☆

Zhengfei Wei [a,*], Prabhakara Rao Bobbili [a,1], S. Senthilarasu [a,c,1], Terry Shimell [b,2], Hari M. Upadhyaya [a,*]

[a] Energy Conversion Laboratory (ECL), Institute of Mechanical, Process and Energy Engineering (IMPEE), School of Engineering and Physical Sciences, Heriot-Watt University, Riccarton, Edinburgh EH14 4AS, UK
[b] Scientific Vacuum Systems Ltd. (SVS), 12 Weller Drive, Hogwood Lane Industrial Estate, Finchampstead, Berkshire RG40 4QZ, UK
[c] College of Engineering, Mathematics and Physical Sciences, University of Exeter, Penryn, Cornwall TR10 9EZ, UK

ARTICLE INFO

Available online 28 October 2013

Keywords:
CIGS solar cells
Up-scaling
Uniformity
Evaporation
Thickness
Heat transfer

ABSTRACT

Substantial efforts have been made globally towards improving Cu(In,Ga)Se_2 thin film solar cell efficiencies with several organisations successfully exceeding the 20% barrier on a research level using the three-stage CIGS process, but commercial mass production of the three-stage process has been limited due to the technological difficulties of scaling-up. An attempt has been made to identify these issues by designing and manufacturing an in-line pilot production deposition system for the three-stage CIGS process which is capable of processing 30 cm × 30 cm modules. The optimisation of the process parameters such as source and substrate temperature, deposition uniformity, flux of copper, indium, gallium and selenium and thickness control has been presented in this investigation. A simplistic thickness distribution model of the evaporated films was developed to predict and validate the designed deposition process, which delivers a comparable simulation compared with the experimental data. These experiments also focused on the optimisation of the temperature uniformity across 30 cm × 30 cm area using a specially designed graphite heating system, which is crucial to form the correct α-phase CIGS in the desired time period. A three-dimensional heat transfer model using COMSOL Multiphysics 4.2a software has been developed and validated with the help of experimental data.

1. Introduction

The development of thin film solar cells has gained significant importance due to better material utilization and reduction of the cost of the modules as compared to c-silicon, in an attempt to achieve grid parity [1–3]. However, there has been fierce competition offered recently by the c-Si technology, which has brought the module cost below $1/Wp [3]. Although, there is good scope for thin film technologies such as CIGS to increase the efficiency and bring the cost down further, it still remains a challenge to scale up the technology to achieve high performance of the modules on a production scale. This mainly stems from the optimisation of the process conditions to achieve control on the morphology and electronic parameters of the thin film layers from batch to batch production. Some organisations have made good progress in transferring state-of-the-art champion cell technologies to industrial production. Solar frontier has achieved 19.7% efficiency on approximately 0.5 cm^2 area CIS solar cell and 14.6% on 125.7 cm × 97.7 cm CIS module efficiency using the two-step process which requires toxic H_2Se vapour [4] for selenisation. Manz has also achieved a CIGS module efficiency of 14.6% with the help of a turn-key production line using the one-step process [5].

This in-line pilot system for high performance CIGS solar cells is the first system of its kind to address the three-stage CIGS process at a production level; a schematic representation of this system is given in Fig. 1. The three-stage process has the potential to yield the highest efficiencies in production as compared with the standard one- and two-step processes, because all of the champion cells are manufactured this way at a research level. However, it is the most difficult of the three processes to scale up. As presented here the pilot production system has a few significant advantages over existing one-step and two-step CIGS production systems.

It has been designed to avoid the use of highly toxic reactant gas H_2Se, which requires robust maintenance of the exhaust and trapping system such as an expensive scrubber along with a gas sensor alarm system to meet the safety standards of the process. In addition, the system also has a built-in flash evaporation unit which can be used to prepare the CdS buffer layer (including a range of alternative Cd free buffers). An obvious advantage lies in utilizing the vacuum deposition process

☆ This manuscript is based on work presented at the Society of Vacuum Coaters 56th Annual Technical Conference in Providence, Rhode Island, April 20-25, 2013.

* Corresponding authors. Tel.: +44 131414381; fax: +44 1314513129.
E-mail addresses: zw60@hw.ac.uk (Z. Wei), h.m.upadhyaya@hw.ac.uk (H.M. Upadhyaya).
[1] Tel.: +44 131414381; fax: +44 1314513129.
[2] Tel.: +44 1189731946; fax: +44 1189731834.

0257-8972 © 2013 The Authors. Published by Elsevier B.V. Open access under CC BY license.
http://dx.doi.org/10.1016/j.surfcoat.2013.10.033

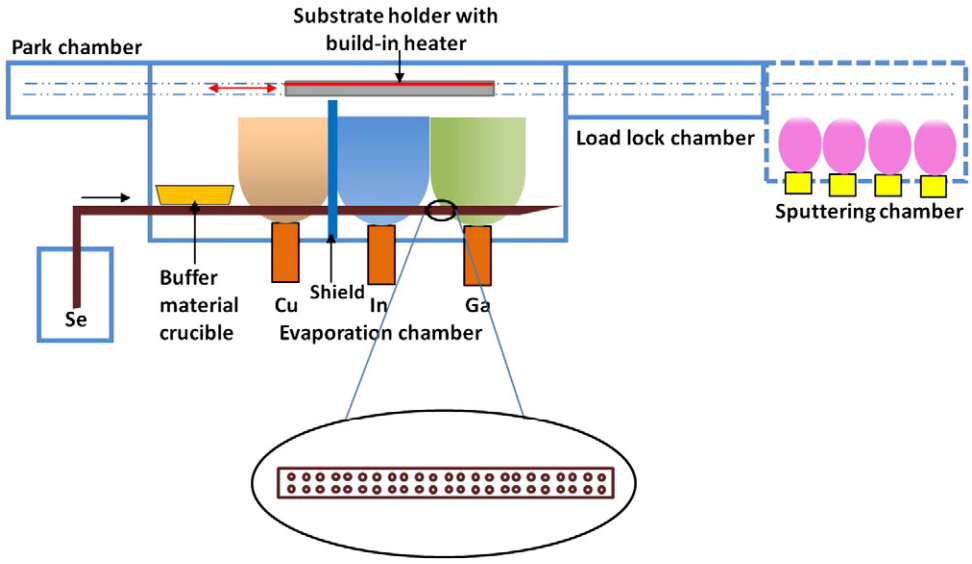

Fig. 1. A schematic of an inline co-evaporation CIGS system.

for all five layer stacks for finishing the CIGS solar cells, thereby reducing the total deposition time, without having to break a vacuum.

The standard system configuration consists of three interconnecting chambers as shown in Fig. 1, comprising a central dealer chamber with an evaporation chamber and sputter chamber connected either side and separately pumped. The substrate loading is controlled by a robotic arm which picks the substrate mounted in a holder from the load lock, and moves it along with the heater to provide local heating of the substrate. The substrate drive is controlled by a servomotor and encoder which allows the substrates to be accurately positioned and oscillate over each of the deposition zones achieving optimum film uniformity. On completion of the process development work, this system has the potential to be developed into an efficient industrially proven process for large scale production of CIGS which will yield a reduction in process time as compared with other energy intensive vacuum apparatus. Normally a significant amount of energy is wasted in breaking vacuum in order to transfer the substrates to perform other vacuum or non-vacuum processes.

Previously the three-stage process had been used to prepare small scale laboratory champion CIGS cells, but to scale up to an industrial level has not been attempted. This is because of several process issues such as heating the substrate to elevated temperatures whilst moving the substrate assembly to different areas of the process chamber for deposition of the various elements and the positioning of multiple deposition sources for each element to achieve uniform distribution of the deposition materials, as well as other process complexities. This in-line pilot system has been developed to grow CIGS layers using a three-stage process on glass substrates to address these scaling issues. In the first stage, the substrate traverses over the In and Ga effusion sources, where (In,Ga)Se is grown on the substrate maintained at 450 °C. In the second stage, the substrate traverses over the Cu effusion source, where $Cu_{2-x}Se$ phase is formed around 550 °C. In the third stage, the substrate is brought back to the In and Ga source zone where CIGS is grown on the substrate to form Cu-poor CIGS around 550 °C. By controlling the movement of the substrate, three-stage deposition process was achieved. It may be noted that a copious amount of Se vapour was used throughout the process. The efforts are underway to optimise the process for large area (up to 30 cm × 30 cm) uniform CIGS thin film deposition on glass substrate, using this machine.

The film uniformity is the key to scaling-up of CIGS solar cells. The thickness and composition uniformity are the primary requirements to achieve good optical and electronic properties for high performance solar cells. From a production point of view, uniformity directly impacts yield [6]. Therefore, for mass production of high efficiency and large area modules, high throughput and reproducible uniformity are crucial. A simple thickness distribution model from two-source evaporation has been developed to simulate the deposition process of each metal source and their thickness uniformity over a large area. This model was used to gain better understanding of the physical system and to predict the film growth. Another important requirement is the flux control which has been addressed as well with the help of the thickness distribution model. In this paper, an attempt has been made towards the development of uniform CIGS layers deposited over a 30 cm × 30 cm area with a specially designed heating assembly. The experiments were designed to validate and test the operational feasibility of an in-line three-stage deposition process. The optimisation was focused on the substrate temperature control and its distribution, which is one of the most important scaling-up requirements. To achieve uniform heating, a thermal model based on the heat transfer module of COMSOL 4.2a was developed and validated with the experimental results.

2. Modelling and experiments

2.1. Thickness and temperature distribution modelling

A simple thickness distribution model from two-source evaporation has been developed using Matlab 2008 to simulate the deposition process of each metal source and its thickness uniformity across a large area. Some process parameters such as source temperature and chamber pressure in the presence of selenium vapour are considered in this model. Besides, a three-dimensional finite-element thermal model was developed for the heat transfer process applied to the substrate with localised heating using COMSOL Multiphysics 4.2a software. The theory, boundary conditions and modelling details for both the parameters are presented in the Results and discussions section.

2.2. Experiments

The in-line pilot scale co-evaporation system (Fig. 1) consists of two deposition zones which are separated by a metal shield [7]. Ga and In sources in the second zone, whilst Cu sources are kept in the first zone. This has been done to avoid cross contamination. The base pressure of the evaporation chamber was maintained at ~10^5 Pa with a processing pressure of ~10^3 Pa. Most of the samples for testing were 5 cm × 5 cm and 10 cm × 10 cm mounted on a graphite substrate holder as shown in Fig. 2. The modelled thickness distribution was experimentally validated. The Cu layer was deposited in the first

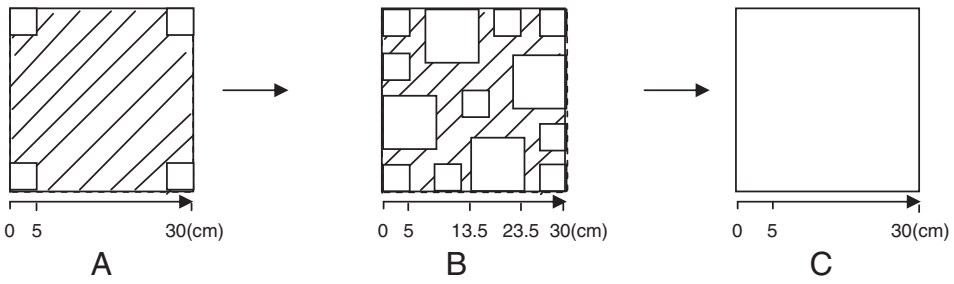

Fig. 2. Masks with capabilities to hold (A) 5 cm × 5 cm, (B) 10 cm × 10 cm and (C) 30 cm × 30 cm substrates for deposition testing of CIGS layers. The white squares in (a–c) are the substrates; the shaded area is un-coated area.

deposition zone on the Mo-coated or bare soda-lime glass (SLG) substrates. The mixture of Ga and In layers was deposited in the second deposition zone. The thickness uniformity was controlled by the temperature of metal sources, temperature of substrates, and the speed of the substrate traverse. The evaporation rate was monitored by in situ quartz crystal microbalance (QCM) sensor built-in with the equipment.

The modelled temperature distribution was also validated with the experimental data. The temperature data was collected by six K-type thermocouples using three designed multi-location stainless steel strips to cover the whole substrate area from the centre to the edge as shown in Fig. 3. There were fifteen points available for selection to mount the six thermocouples per run. Enough care was taken to ensure that proper contact between the thermocouples and glass substrate was made by providing tension to the thermocouples. White ceramic layers were positioned between the three stainless steel straps so the holder can withstand temperatures of up to 800 °C, which was used to avoid heat transfer from the chamber body to the thermocouples. The data was collected through 16-Channel thermocouple input module (National Instruments) installed with a LabVIEW programme.

3. Results and discussions

3.1. Thickness distribution model of evaporation process

Inside the system for high efficiency CIGS solar cells, the thickness uniformity for each elemental source in the *x*-direction (along the movement of the substrates) and in *y*-direction (perpendicular to movement of the substrates), determines the final CIGS layer thickness and composition uniformity. Therefore, depositing uniform film thickness from each elemental source is the primary objective. Specifically, in *x*-direction, there is only one source for each metal element; the uniformity is mostly dependent on stability of the substrate speed and evaporation rate. In the *y*-direction, there are two point effusion sources for each metal element, and they are heated by two separate DC power supplies. Fig. 4 describes the geometrical positioning of these elemental pair sources to ensure the better overlap of elemental flux resulting in good uniformity of the layers.

A preliminary mathematical model to describe the thickness distribution of the evaporation process of metals viz. Cu, In and Ga was developed. The validity of the model was restricted to the particular source design and acceptable stabilised evaporation temperatures. To reduce complexities of calculations and modelling, the following assumptions were made.

(1) It was assumed that the pair of the sources for each element was heated to the same evaporation temperature throughout the required deposition period.
(2) The change in the chamber pressure during the deposition was neglected.
(3) The deposition area was differentiated into small enough elements to be integrated.
(4) The heating of substrate didn't lead to the changes on the source temperature.
(5) The effects of mass losses of the sources after every deposition on the deposition profile were neglected.

To achieve good thickness and composition uniformity, it requires the optimised geometrical source design and the source operational temperature profile. A proper estimation of each source evaporation rate and deposition distribution is also needed. Hence, the source evaporation and deposition model was developed to propose the dynamic condition which allows analysing thickness uniformity of the deposited layers.

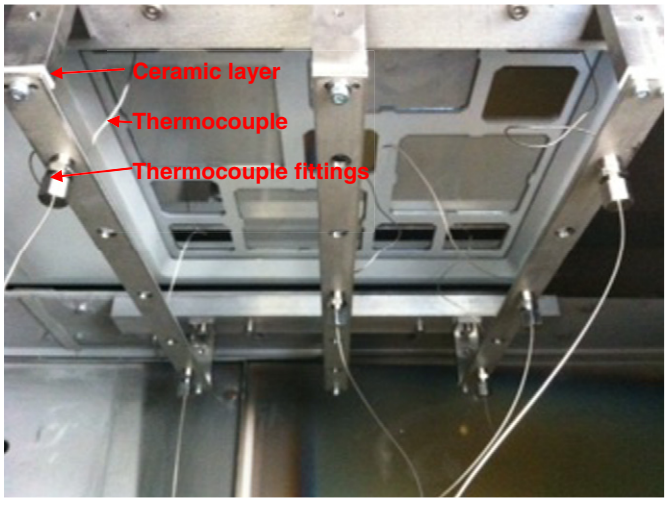

Fig. 3. Six thermocouples positioned underneath the glass substrate mounted on a movable heater stage assembly.

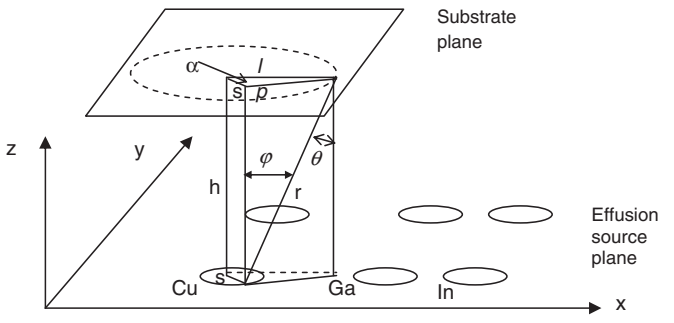

Fig. 4. Geometry of evaporation and deposition model.

3.1.1. Mathematical model for the evaporation and deposition process

The evaporation theory [8] and semi-empirical models [9,10] provide a fundamental understanding of the principle and mechanism of the deposition process as it applies to effusion sources and thickness-uniformity distribution. This model involves the problems concerned with the metals operated at high temperatures. The vapour pressure and rates of evaporation are essential in order to interpret the results observed and predict the possible optimisation changes. As shown in Fig. 4, a Cartesian coordinate system (x, y, z) is used to define the locations and geometry of the whole deposition system. h is the source-to-substrate distance, s is the radius of the mouth of the source crucible, l is the radius of a circular deposition pattern, and α is the angle between l and the projection of s on the substrate plane. The evaporation rate F represents the volume of the molecules striking the unit area per unit time [8], this can be described as:

$$F = (P_{sat}(T) - P_{cham})\sqrt{\frac{M}{2\pi RT}} \tag{1}$$

where R is the ideal gas constant, T is the vapour temperature, M is the molar mass of the evaporated material, $P_{sat}(T)$ is the saturation pressure of the material which is derived according to Hanket's method [11] as:

$$\log P_{sat}(T) = A - \frac{B}{T} \tag{2}$$

where A and B are constant. P_{cham} is the partial pressure in the chamber. Thus, the thickness d received from a small disc source [8] can be given by:

$$d = \iiint_{t,s,a} \frac{Fsd\alpha ds}{\pi\rho}\frac{h^4}{r^4}dt \tag{3}$$

where t is the deposition time, ρ is the density of the material, and r is the deposition radius. Integrating α from 0 to 2π and as $r^2 = h^2 + l^2 + s^2 - 2ls\cos\alpha$, the resulting expression of d [8] is

$$d = \iint_{t,s} \frac{2Fh^2}{\rho}\frac{h^2 + l^2 + s^2}{\left[(h^2 - l^2 + s^2) + (2lh)^2\right]^{l,s}} sdsdt. \tag{4}$$

The deposition from two Cu sources at a point on the substrate is calculated by the sum of the thicknesses from two individual sources.

3.1.2. Simulation results and experimental validation

Fig. 5A shows the simulated Cu fluxes in the y-direction, which determines the thickness distribution over the substrate. Fig. 5B shows the experimental results of the Cu deposition carried out at room temperature and its comparison with simulated data. The modelling results show non-uniformity mainly at the edges of the 30 cm × 30 cm substrate geometry, which corresponded with experimental results as shown in Fig. 5B. The non-uniformity of the films at the edges was ± 13%, which is an acceptable value for deposition onto the substrates at room temperature. The non-uniformity between centre and edge has been reported to decrease with the increase in substrate temperature [12], which was observed in subsequent experimental trials.

Based on the validation of the Cu (Fig. 5B) deposition model over 30 cm × 30 cm area, it was assumed that the evaporation and deposition model was extended for In and Ga deposition as well. The multiple source (Cu, In and Ga pair sources) deposition onto the substrates at room temperature showed similar behaviour of thickness variation across the specified area of the substrate which corresponded with the simulation results as shown in Fig. 6. In this experiment, the substrates were located evenly on nine positions across the centre to the edge of the 30 cm × 30 cm area as shown in Fig. 2b. The measured non-uniformity was comparable with the simulated results. The non-uniformity was more pronounced at the edges along the y-direction, which was confirmed previously with Cu-source experiment as shown in Fig. 5B. The non-uniformity of the films at nine selected positions was ± 8%.

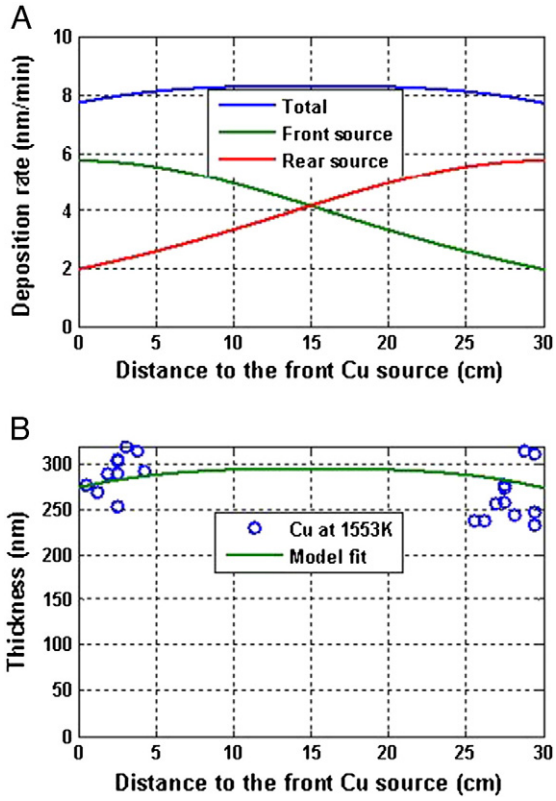

Fig. 5. (A) Modelled deposition rate of two copper sources at 1553 K in the y-direction. (B) Measurements of Cu-coated four 5 cm × 5 cm samples and model-fit for film thickness.

3.1.3. Simulations on the effects of source temperature and chamber pressure in presence of selenium

The source temperature is considered as the most important variable in an evaporation process. The deposition rate of each effusion source was controlled by changing the source temperature at the same chamber pressure around ~10^5 Pa. The simulated deposition rates for copper, indium and gallium were calculated near the

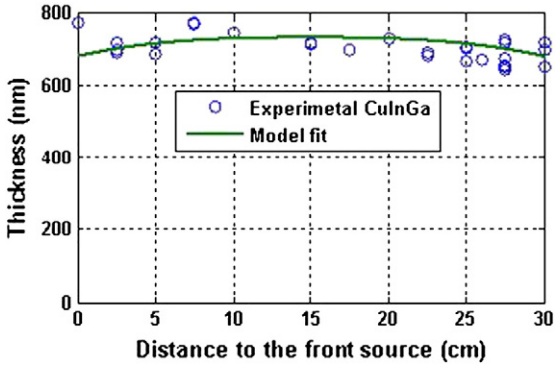

Fig. 6. Thickness measurements of CuGaIn-coated nine 5 cm × 5 cm samples and model-fitted film thickness. In this deposition run, Cu, Ga and In source temperatures were at 1568 K, 1248 K and 1168 K respectively.

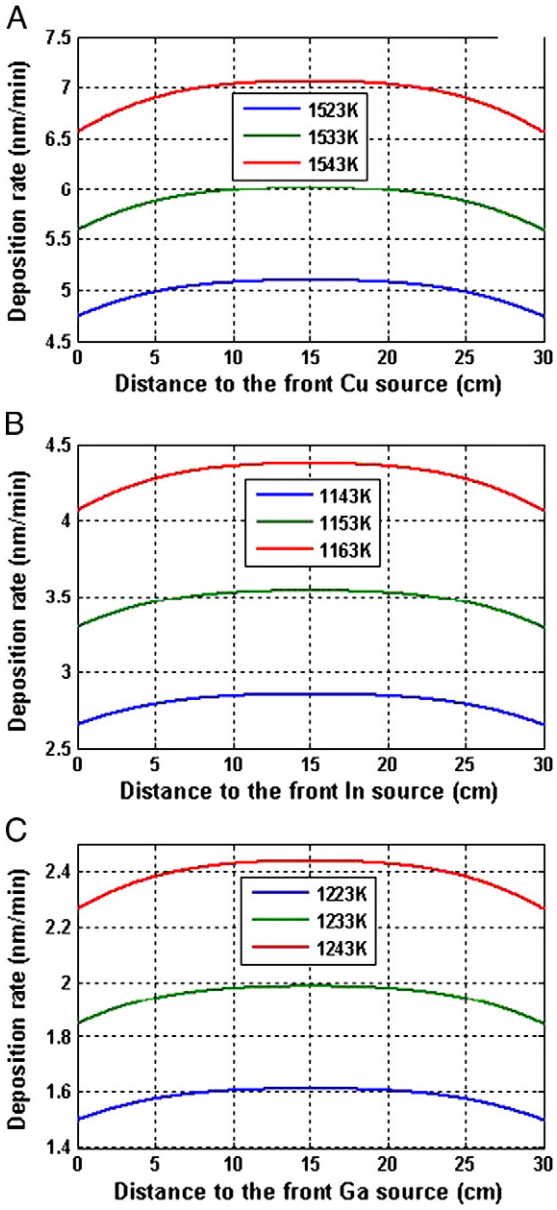

Fig. 7. The variation of the deposition rate at different temperatures of (A) copper source, (B) indium source and (C) gallium source.

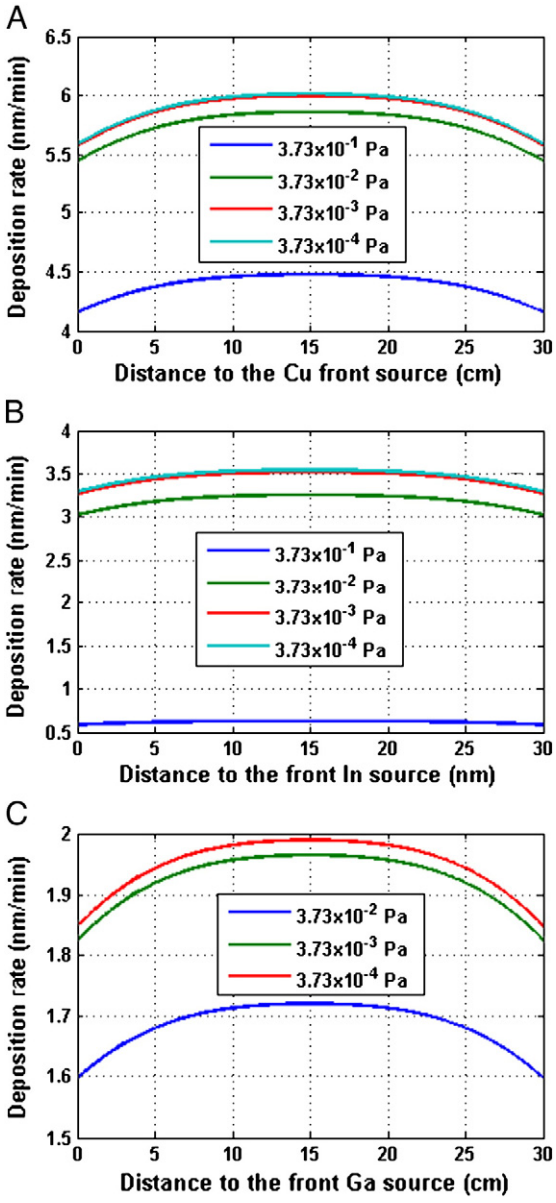

Fig. 8. The variation of the deposition rate at different chamber pressures of (A) copper source at 1553 K, (B) indium source at 1153 K and (C) gallium source at 1233 K.

evaporation temperatures as shown in Fig. 7. This was used to fine tune the deposition rate in order to achieve good reproducibility. It was found that the change of the deposition rate was proportional to the change of the source temperatures for all Cu, In and Ga.

The pressure of the chamber is found to be another important parameter in determining the deposition rate of copper, indium and gallium sources which are shown in Fig. 8. These results are useful to predict the evaporation rate variation after selenium vapour was introduced into the chamber. The presence of selenium vapour can increase the chamber pressure. A decrease in the deposition rate was observed as the chamber pressure increased for all these Cu, In and Ga sources. It showed the same trend for all three metal sources. When the chamber pressure was larger than 10^{-5} Pa, there was no significant change on the deposition rate whilst keeping the same source temperature. For gallium source, at 10^{-2} Pa the calculated deposition rate was negative which indicates no evaporation taking place [8], hence the deposition rate curve could not be generated in Fig. 8C.

3.2. The temperature distribution model for heat transfer process

The temperature distribution model is a thermal model based on heat transfer effect mainly determined by radiation and conduction process. In this model, the convection effects were not considered. The radiation covers heat transfer a) between the heater and substrates, and b) from the external surface of the heater and substrates to the surrounding environment. The conduction was considered between the substrate holders and different pieces of the substrates. The typical calculation by COMSOL is quite complex and time consuming. The following assumptions were made to simplify these computational problems.

(1) It was assumed that there is good heat transfer efficiency between heater and the substrates.
(2) It was also assumed that the substrate edges and the graphite substrate holder were in good thermal contact.
(3) The heat radiation to the internal surface of the heater assembly was neglected due to the proper insulation from the graphite holder.

(4) All the surfaces were opaque and radiated diffusively.
(5) The chamber was assumed as a blackbody at room temperature.
(6) The power input on the heater was stabilised during the process.

3.2.1. Mathematical model of heat transfer process

This model is based on heat transfer principle, which is defined as the movement of energy due to the difference in temperature. In order to achieve high process temperature uniformity on glass substrate in a short period, the graphite radiation heater was selected in this system. The heat transfer mechanisms by radiation take place through the transport of photons. The first law of thermodynamics governs all heat transfer, which is known as the principle of conservation of energy. A simplified form of heat equation [4] is:

$$\rho C_p \frac{\partial T}{\partial t} + \rho C_p u \cdot \nabla T = \nabla \cdot (k \nabla T) + Q \tag{5}$$

where ρ is the density, C_p is the specific heat capacity at constant pressure, T is the absolute temperature, u is the velocity vector, Q represents the heat flux from the heat sources, and k is the thermal conductivity.

The total heat flux vector [4] is defined as:

$$Q_t = \nabla \cdot q_t = \nabla \cdot (\rho u U - k \nabla T + q_r) \tag{6}$$

where Q_t is the total heat flux from the heat source, q_t is the total heat flux, q_r is the radiative heat flux, and U is the internal energy.

For the heat transfer process, the heat fluxes and sources at the domain and boundary were computed respectively with the consideration of different physical variables. For domain heat flux, two main types of heat fluxes were considered: conductive heat flux in solid material under consideration and radiative heat flux from the non-conductive graphite heater. The domain heat fluxes can be derived from Eq. (6), which are also available as boundary heat fluxes. The boundary heat fluxes are normally equal to the mean value of the adjacent domain such as the graphite heater and substrate holder. The radiative heat flux on boundaries [4], r_{flux}, is a scalar quantity highlighted as:

$$r_{flux} = \varepsilon\sigma\left(T_{amb}^4 - T^4\right) + \varepsilon\sigma\left(G - T^4\right) + q_w \tag{7}$$

where the terms respectively account for surface-to-ambient radiative flux, surface-to-surface radiative flux and radiative in participating net flux, q_w. ε is known as surface emissivity, σ is the Stefan–Boltzmann constant, T_{amb} is the ambient temperature, and G is the total arriving radiative flux.

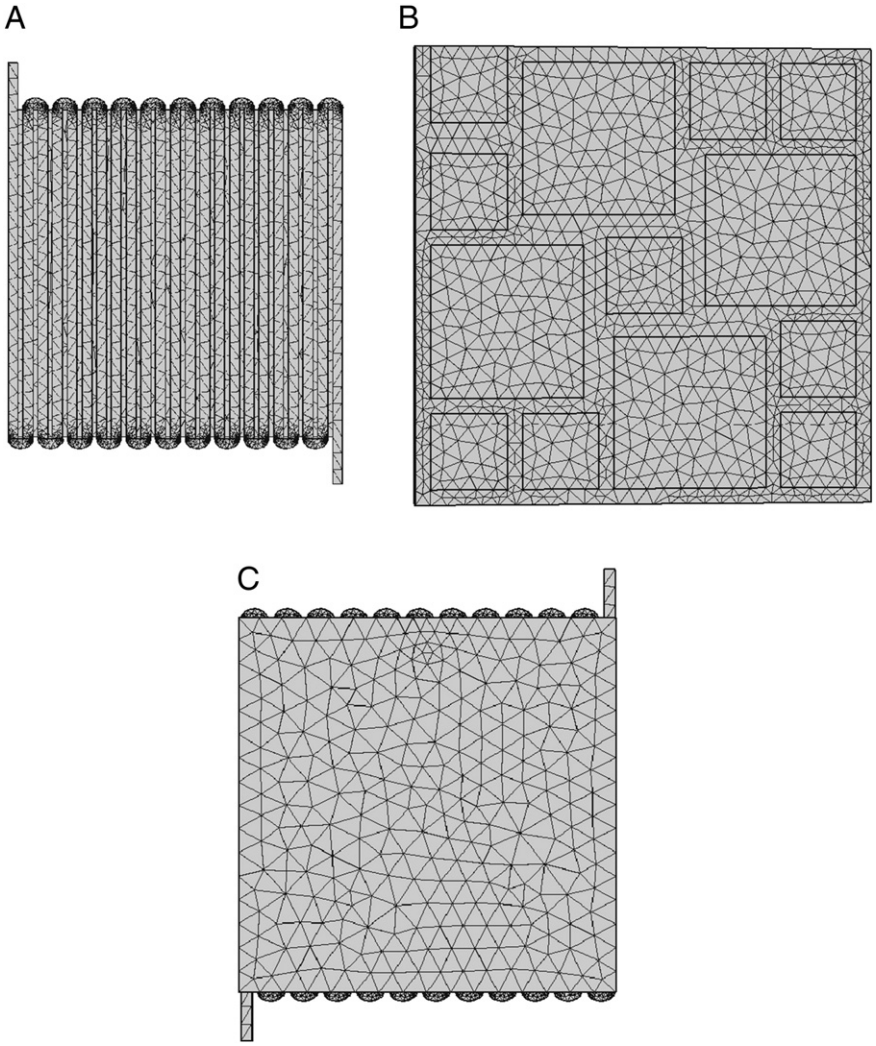

Fig. 9. Bottom view of the mesh elements of heating assembly and substrates: A) top view of heater elements, B) bottom view of the 5 cm × 5 cm and 10 cm × 10 cm-sized SLG substrates with a graphite holder, and C) bottom view of the 30 cm × 30 cm-sized glass substrate.

In this model, surface-to-surface radiation [4] can be described as the generalised equation of Eq. (6):

$$G = G_m + F_{amb}\sigma T_{amb}^4 \quad (8)$$

where G_m is the mutual irradiation arriving from other surfaces in the simulated geometry, and F_{amb} is the ambient view factor.

3.2.2. Simulation results and experimental validation

COMSOL software was used to solve the above heat transfer equations. The simulation of the temperature distribution was performed on bare soda-lime glass. COMSOL uses the proven finite element method (FEM) to solve the models with adaptive meshing. Three-dimensional (3-D) meshes were built with the sufficiently fine resolution to obtain an accurate solution as shown in Fig. 9.

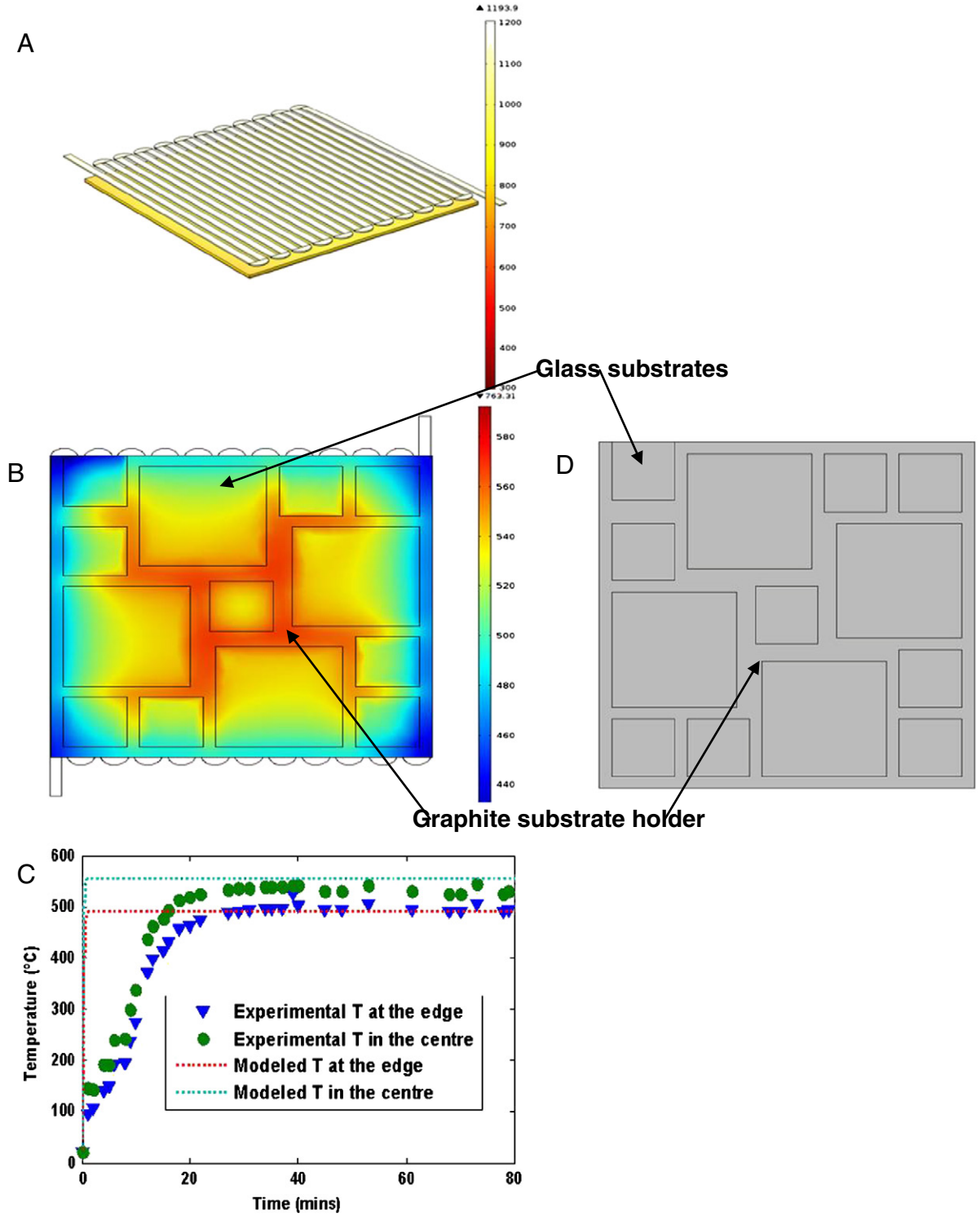

Fig. 10. Simulated temperature distribution on nine 5 cm × 5 cm and four 10 cm × 10 cm substrates across 30 cm × 30 cm-area with a specially designed graphite heater: (A) top view of the heater assembly, (B) bottom view of substrate temperature distribution, and (C) simulated and experimental temperature distributions on the 30 cm × 30 cm substrate using a specially designed graphite heater for 80 min. (D) the glass substrates and the graphite substrate holder configurations.

The results of a 3-D temperature profile and distribution on 30 cm × 30 cm substrate with a specially designed graphite heater were calculated and presented in Fig. 10. It shows quite good uniformity with temperature variation around 50 °C. The non-uniformity appears mainly at the four corners of the graphite substrate holder recording the lowest temperature readings, with the highest temperature measurement recorded in the centre. This may be due to the mismatch of the thermal conductivity of the graphite and soda-lime glass (SLG).

In order to form proper α-phase CIGS alloy, the substrate requires to be heated up to more than 500 °C for a certain period of time, depending on optimisation conditions set by various groups [1,13,14]. This requires the stabilised power output from the heater and flexible control on the fine tuning of temperature changes. A heater assembly system (Fig. 3) was used to carry out the temperature profiling measurements. The simulated and experimental temperature distributions were compared across 30 cm × 30 cm area with nine evenly positioned 5 cm × 5 cm soda-lime glass substrates. The experimental data was the average of four thermocouples at four different locations. The non-uniformity of bare SLG substrates heated by the specially designed graphite heater was reduced to ±5% across the 30 cm × 30 cm area as shown in Fig. 10. This provides a very promising solution towards the uniform heating of large area applications. In Fig. 10B, the small squares are glass substrates, which are held by a graphite holder. They were labelled in Fig. 10B and D. The values from Fig. 10B are obtained from the simulated results. The temperature variation on the glass substrates were measured within 50 °C. The temperature difference between graphite substrate holder and the glass substrates were large than 50 °C, this may be due to high thermal conductivity of the graphite. There was a discrepancy between the simulation and experimental data for the initial 15 min of heating. The simulated results were showing quick ramp-up time compared to the experimental measurement. This may be due to the following reasons:

1) Outgassing effect from the heater assembly can lead to overall pressure increases in the main chamber, which slows down the initial heating performance.
2) The accuracy of measurement of the K-type thermocouples may not be good enough at the temperature range between 20 to 500 °C.
3) The contact between the control thermocouple of the PID controller and SLG edge may not be proper.
4) The boundary conditions of heat transfer model need to be improved especially the 'surface-to-ambient' to fit into the real heating process.

Based on the progress made using the graphite heater, a heat trial was performed to test the temperature distribution on a single piece of 30 cm × 30 cm glass substrate. This was a very important step to investigate the solution of overcoming the scaling up challenge. In Fig. 11, the temperature on the 30 cm × 30 cm substrate distributes in a rippled contour shape. It shows good uniformity at the central part of the substrate, but it appears lower at the corners. This leads to a non-uniformity of approximately ±5%.

The experimental results were in a good agreement with the simulated results. The experimental data was the average of four thermocouples at four different locations of the edge in Fig. 11B. A similar heating profile was observed for both the separate glass substrates and the graphite holder. Further, better contact could be ensured on the single piece of 30 cm × 30 cm area substrate. However, the experimental temperatures during the initial 15 min were lower than the simulated temperatures, which were discussed previously. Due to simplified modelling assumptions, there was an ambiguity in temperature rise that results from experimental results. The equilibrium temperature was lagging behind by 15 min compared with the simulated results. It was observed that the single piece of glass was deformed as shown in Fig. 12. It can be seen that the centre of the glass buckles slightly. This may be due to the gravity of the glass when the melting temperature of the glass was reached, then it starts to flow. It may also be caused by the non-uniform heating experienced at the edge from the heater.

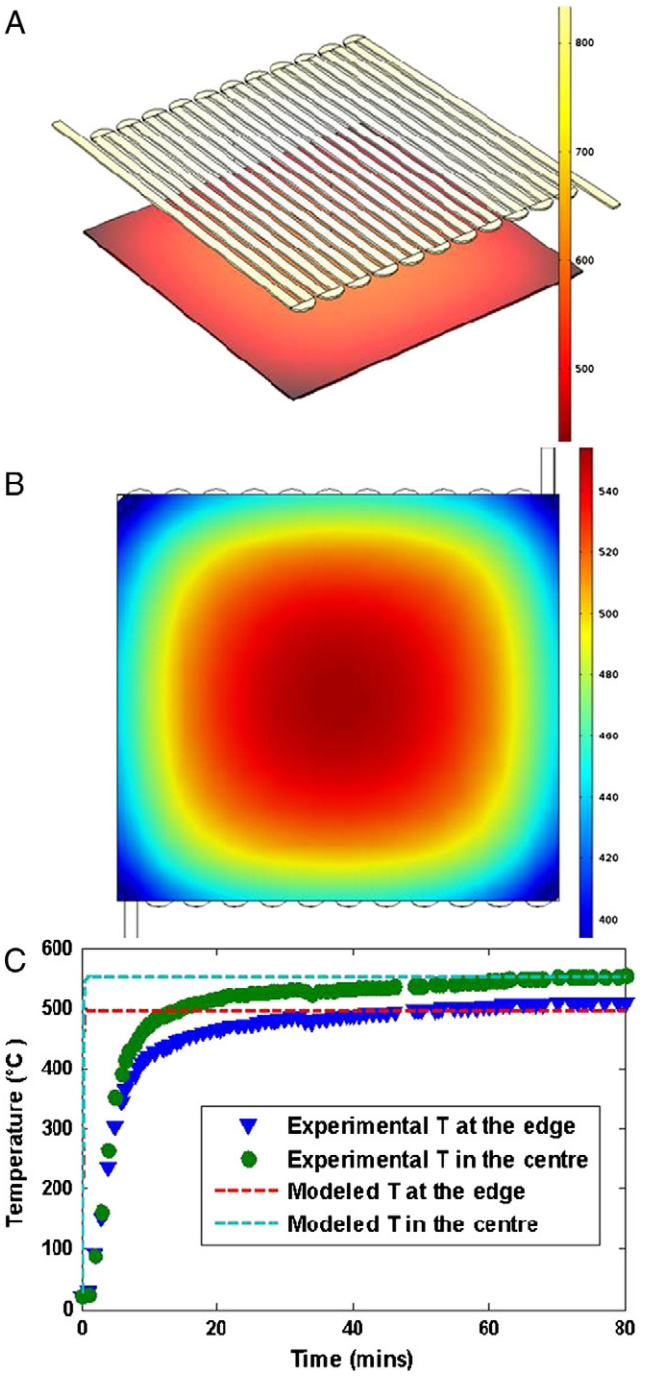

Fig. 11. Simulated temperature distribution on a 30 cm × 30 cm-area glass substrate with a specially designed graphite heater: (A) top view of the heater assembly, (B) bottom view of substrate temperature distribution, and (C) simulated and experimental temperature distributions on the 30 cm × 30 cm substrate using a specially designed graphite heater for 80 min.

A combination of redesigning the heater reflector to improve the temperature uniformity at the edges is planned to overcome this problem in the future. An improved substrate holder design, changing the orientation of the substrate assembly and repositioning of the thermal sources, may be required when increasing the substrate area as used for standard 120 cm × 60 cm modules.

Towards the large area CIGS module fabrication, the necessary control of parameters viz. temperature uniformity, composition uniformity and thickness uniformity is essential. In this current study, the above control parameters have been limited to 30 cm × 30 cm area with the current in-line tool. This pilot scale in-line system provides confirmation

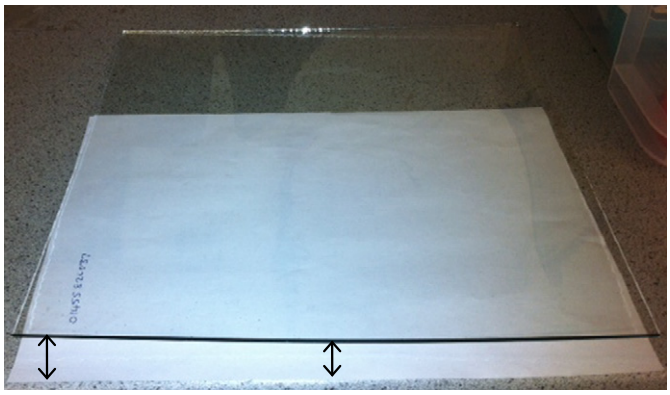

Fig. 12. The photograph shows the buckling of 30 cm × 30 cm area glass substrate.

from our results that the temperature controls over 120 cm × 60 cm modules will be much more challenging. However, we have some strategies in place to modify the heater design to tackle this challenge, which will be discussed elsewhere. To achieve the composition uniformity over large module area, the movement of substrate holder in the two zones will be the critical controlling factor, which will be optimised along with the effusion source control. The thickness control over 120 cm × 60 cm area is also critical to the quality and performance of the CIGS solar cells. The thickness over the large area deposition for standard 120 cm × 60 cm module area, and linear sources may be designed to gain the thickness uniformity control instead of multiple point sources.

4. Conclusion

This work was conducted to investigate the challenges on the process optimisation for large area high performance CIGS solar cells. Two scaling up challenges were targeted in this paper. The first one was the Cu, In and Ga layer thickness uniformity over 30 cm × 30 cm area, deposited using an in-line evaporation system, which was predicted and validated using a simple evaporation model. These results were in alignment with the predicted data leading to a thickness uniformity of ±8%. The second challenge was the uniform temperature distribution over a 30 cm × 30 cm area substrate, which was heated using a specially designed graphite heater. Temperature mapping was conducted using K-type thermocouples and the simulated results were calculated using a 3D heat transfer model. The experimental and simulated results were complementary, which resulted in non-uniformity of ±5% from centre to edge across a 30 cm × 30 cm area. The results of this investigation provide a promising solution towards uniform heating of a 30 cm × 30 cm area for high performance solar cell application.

Acknowledgements

This research work was supported partially through the funding support received from EPSRC UK–India programme APEX (EP/H040218/1) and partially supported by Excitonic Supergen (EPSRC (EP(G03101088/1)) programme.

References

[1] I. Repins, M.A. Contreras, B. Egaas, C. DeHart, J. Scharf, C.L. Perkins, B. To, R. Noufi, Prog. Photovolt. Res. Appl. 16 (2008) 235–239.
[2] P. Jackson, D. Hariskos, E. Lotter, S. Paetel, R. Wuerz, R. Menner, W. Wischmann, M. Powalla, Prog. Photovolt. Res. Appl. 19 (2011) 894–897.
[3] Z.M. Beiley, M.D. McGehee, Energy Environ. Sci. 5 (2012) 9173–9179.
[4] http://www.solar-frontier.com/eng/news/2013/C020760.html19/09/2013.
[5] http://www.manz.com/media/news/archive/2012/manz-presents-cigs-world-record-module-with-efficiency-of-146-at-pv-taiwan-42519/09/2013.
[6] H. Sugimoto, Y. Kawaguchi, Y. Yasaki, T. Aramoto, Y. Tanaka, H. Hakuma, S. Kuriyagawa, K. Kushiya, 26th European Photovoltaic Solar Energy Conference and Exhibition, Hamburg, Germany, 2011, pp. 2307–2310.
[7] Z. Wei, T. Shimell, H.M. Upadhyaya, 26th European Photovoltaic Solar Energy Conference and Exhibition, Hamburg, Germany, 2011, pp. 2840–2844.
[8] R. Glang, in: L.I. Maissel (Ed.), Handbook of Thin Film Technology, McGraw-Hill Book Co., New York, 1983, pp. 1–87.
[9] G.M. Hanket, P.D. Paulson, U. Singh, S.T. Junker, R.W. Birkmire, F.J. Doyle, E. Eser III, W.N. Shafarman, Photovoltaic Specialists Conference, 2000. Conference Record of the Twenty-Eighth IEEE, 2000, pp. 499–504.
[10] K. Mukati, B.A. Ogunnaike, E. Eser, S. Fields, R.W. Birkmire, Ind. Eng. Chem. Res. 48 (2009) 5975–5991.
[11] G.M. Hanket, R.W. Birkmire, S. Fields, E. Eser, Photovoltaic Specialists Conference (PVSC), 2010 35th IEEE, 2010, pp. 000770–000775.
[12] C. Guillén, J. Herrero, Sol. Energy Mater. Sol. Cells 73 (2002) 141–149.
[13] A. Chirilă, S. Seyrling, S. Buecheler, D. Guettler, S. Nishiwaki, Y.E. Romanyuk, G. Bilger, A.N. Tiwari, Prog. Photovolt. Res. Appl. 20 (2012) 209–216.
[14] R. Caballero, C.A. Kaufmann, V. Efimova, T. Rissom, V. Hoffmann, H.W. Schock, Prog. Photovolt. Res. Appl. 21 (2013) 30–46.